Filled Resist Systems

Thomas Hanemann[1,2], Claas Mueller[1], Michael Schulz[1,2]
[1]Department of Microsystems Engineering (IMTEK), University of Freiburg, Georges-Koehler-Allee 102, D-79110 Freiburg, Germany
[2]Institute of Materials Research, Forschungszentrum Karlsruhe, PO-Box 3640, D-76021 Karlsruhe, Germany

Keywords:
lithography, nanofiller, LIGA, SU-8, microstereolithography

Abstract:

Content

1. Introduction 3
2. Variants of lithography 4
2.1 UV lithography 5
2.2 Deep x-ray lithography 5
2.3 E-beam lithography 6
2.4 Microstereolithography 7
3. Properties of Filler-Polymer Matrix-Composites 8
3.1 Flow properties 9
3.2 Optical properties 12
4. Application of filled resist systems 13
4.1 Nanoparticle filled resists for e-beam lithography 13
4.2 Filled preceramic polymers 14
4.3 Filled SU-8 resists 20
4.3.1 Electrical conductive SU-8-composites 20
4.3.2 Magnetic SU-8-composites 21
4.3.3 Silica filled SU-8 for microelectronic applications 21
4.3.4 Lithographically-anchored nanoparticle synthesis (LANS) 21
4.3.5 SU-8-alumina-composites 21
4.4 Filled resists for microstereolithography 24
5 Miscellaneous 28
5.1 Photosensitive polyimide/silica composites 28
5.2 Water based filled photoresists 29
5.3 Three dimensional lithography using sol-gel based compositions 30
6 Summary 30
7 Acknowledgement 30
8 References 31

1. Introduction

All modern lithographic methods in microelectronics and microsystem technologies are based on the interaction of photosensitive monomers, oligomers and polymers with electromagnetic radiation. The kind of photoreaction, which depends strongly on the chemical and physical properties of the used resist material as well as on the applied radiation type and energy, determines the application possibilities. Different photoreactions like photopolymerization, photocrosslinking, photodegradation and photo-thermal reactions have been described in literature [Peif1997]. With respect to lithography photopolymerization and photodegradation are the most important ones. If a monomer or oligomer polymerizes under irradiation conditions independently from the applied wavelength, the material is defined as a negative resist, i.e. a negative image of the pattern on the used mask will be created. If a polymer is destroyed by light via chain scission the material behaves as a positive resist (Fig. 1). Both mechanisms are exploited in the realization of electronic and printing materials, device fabrication in microelectronics and microsystem technology, packaging as well as in different surface modification techniques for a post processing of films, textiles or fibers [1].

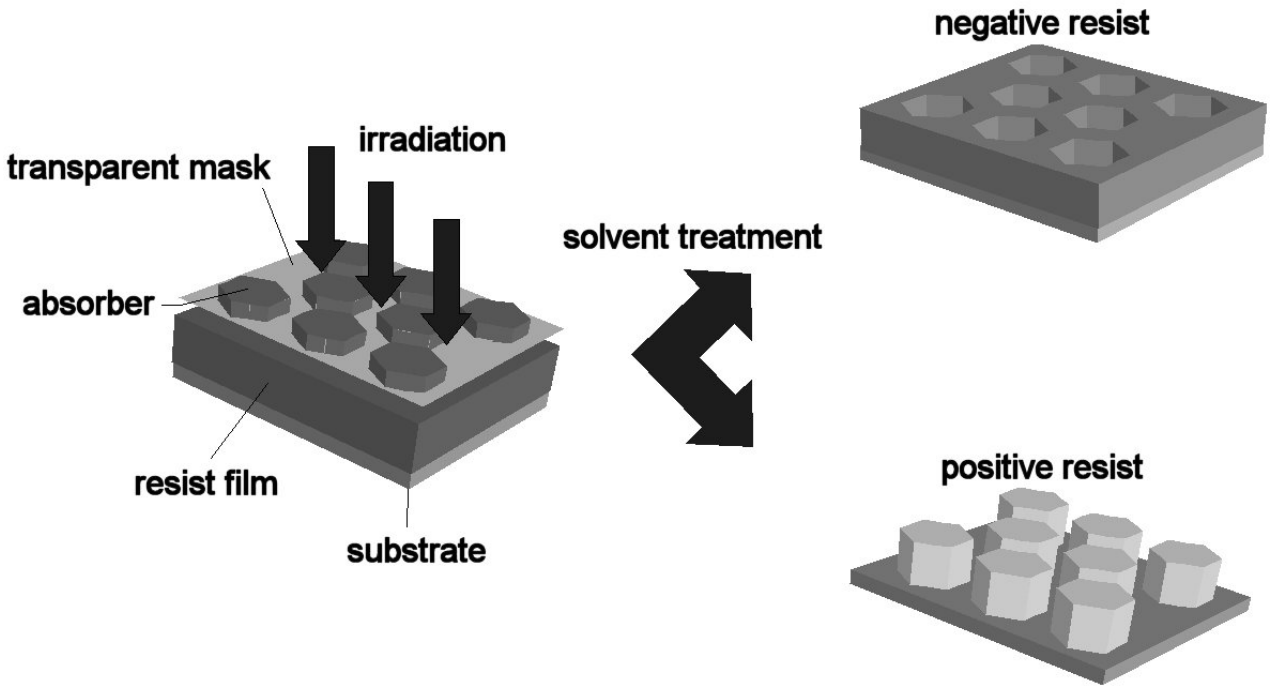


Fig. 1 Principal resist behaviour during irradiation

With respect to a further miniaturization of the aspired micro- and nanostructures with variable aspect ratios in combination with a further progress in the different established lithographic methods and new developments like laser lithography in the deep UV-range new resist systems have been developed in the last years [2-4].

The addition of ceramic or metal fillers to photoresists is motivated by the following aspects:

- improved sensitivity against electromagnetic radiation
- better resolution
- improved chemical and mechanical resist stability
- introduction of new functionalities (electrical conductivity, magnetic properties)
- direct fabrication of ceramic or metal microcomponents using the lithographic microstructuring in combination with a thermal post processing (debinding and sintering)
- rapid prototyping of ceramic and metal parts.

2. Variants of lithography

In microelectronics and microsystem technology three fundamental lithographic techniques have been established in the last years. For a long period of time mercury vapour arc lamps were used for the photolithography in the visible or near UV-range, powerful laser sources in combination with special chemical amplified resists enables today the UV-lithography in the UV- and deep UV-range down to the realization of 100 nm structures [2,3]. High aspect ratio microstructures can be realized via deep x-ray lithography. Geometric details in the nm-range can be generated via electron beam lithography, which is essential for the optical mask fabrication. Due to the shadow projection principle the above mentioned lithography variants allow only the patterning of 2.5D structures.

Real 3D-microstructures can be fabricated via microstereolithography due to the layer by layer irradiation of a negative resist using a dynamic mask generator. In the following the fundamental principles and the requirements for the applied resist materials are described.

2.1 UV lithography

The UV lithography is an optical lithography technology for wavelengths of 365 nm or shorter and is already widely used for the fabrication of microsystems and advanced CMOS components. The lithography process transfers a pattern from a mask to an photo resist. First the substrate is coated with a photo resist, a material which is sensitive to UV-light. This is normally done by dropping the resist on top of the substrate which is then spun at a high speed to get a uniform thick resist layer. The substrate with the resist is then exposed to UV-light through a mask that protects parts of the resist. Finally the substrate is put in a developer. SU-8 is a typical example for a negative resist and is widely used for the fabrication of high aspect ratio structures. SU-8 components are useful for MEMS, fluidic and packaging applications. There are also two different ways to expose the resist to UV-light, shadow exposure and projection exposure. In the shadow exposure the sample is put in contact or close contact (called proximity exposure) to the resist and the pattern will be directly transferred to the resist with a scale 1:1. In a projection exposure the mask and pattern are more separated and the optical system has a magnification up to 10. The consequence of the magnification of the optical system is the possibility to have a mask demagnification ratio, which makes the mask fabrication easier.

2.2 Deep x-ray lithography

To prevent the synchrotron radiation from being absorbed on its way from the bending magnet to the sample, the lithography beamline is highly evacuated. Separated by a beryllium window and a shutter the concluding scanner chamber is evacuated and flooded with 100 mbar helium after the sample is mounted. In the scanning chamber the sample holder, carrying the mask and the resist coated substrate, is moved up and down in front of the beam (Fig. 2) [3].

The X-ray scanners used allow for the exposure of sample areas up to 10 cm^2. Since large angle deflection of the synchrotron radiation is not possible the substrates must be fixed vertically in the scanner. These boundary conditions influence the resist material working properties. After the coating of the substrate a drying step is required. No volatile fractions are allowed to prevent the chamber from damage and the resist must not be liquid because of the vertical mounting.

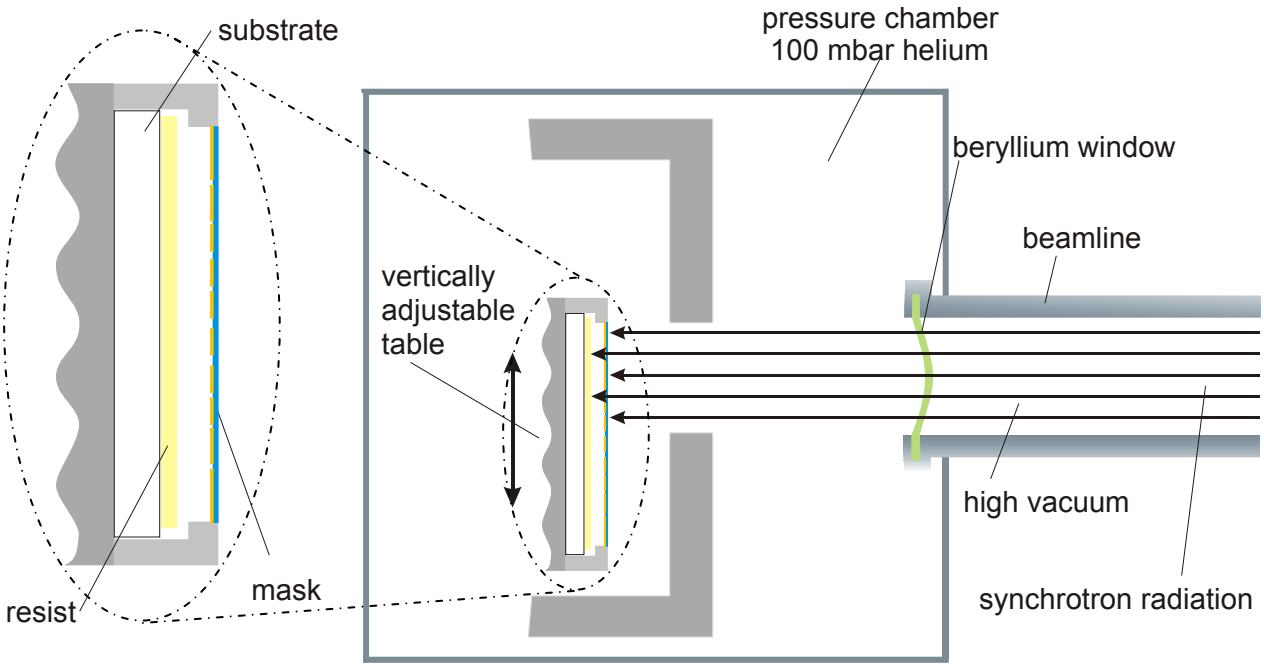


Fig. 2 Scheme of a X-ray scanner according to [3]

A specific range can be extracted from the synchrotron spectra by using appropriate filters in the beamline whereby the gradient between top and bottom dose can be adjusted, too. The calculation of the exposure dose needed is based on the radiation source parameters, the filters and windows in the beamline as well as the atomic composition and resists density.

The absorption of X-ray in matter is caused by interactions between photons and electrons [4]. Emerging scattered radiation and pair formation effects are not taken into account for the resist change. Based on the values of the mass absorption coefficient the absorption of the resist material can be calculated following the empirical formula (1) with the mass absorption coefficient σ, a wavelength dependent constant $c(\lambda)$, the material density ρ, the atomic number Z and the used wavelength λ [5].

$$\sigma = c(\lambda)\cdot\rho\cdot Z3\cdot\lambda 3 \qquad (1)$$

2.3 E-beam lithography

Nanoscale structures can be generated using e-beam lithography (EBL). EBL is used for either mask generation or direct writing of patterns on the wafer. Most direct write systems use a small electron beam spot that is moved with respect to the wafer to expose the pattern one pixel at a

time. Therefore the systems can be classified as raster scan or vector scan with fixed or variable beam geometries, respectively. After generation from a cathode the electrons are accelerated and focused by electrostatic lenses and a variety of apertures and knife edges [3,4].

When electrons penetrate the resist layers, they are scattered and therefore experience a deviation from their original direction. Depending on the electron energy and the atomic mass the angle of deviation varies. The large atomic mass of the substrates causes so called back scattering leading to exposure of the resist from underneath in areas which are not supposed to be irradiated.

Forward scattering of the electrons on the atoms of the resist leads to a strong broadening of the beam. These proximity effects are a major challenge in EBL [3,4].

2.4 Microstereolithography

Microstereolithography was the first rapid prototyping process in microsystem technologies. Rapid prototyping has been established in the macro- and for some years now in the microworld for a rapid product development with respect to a significant reduction of the time-to-market-factor and the product development costs. A comprehensive overview about Rapid Prototyping in micro- and nanotechnology can be found under [6]. Microstereolithography was developed in the early nineties of the last century using a photocurable resin as a negative resist material and a xenon discharge lamp or an Ar-ion-laser as light source fabricating a simple microfluidic systems or a microclamping tool [7,8]. The smallest geometric features were in the µm-range, aspect ratios around ten and more could be achieved. The original stereolithography technique was invented in 1984 by 3D systems [9]. In opposite to shadow mask based lithographic techniques the 3D-microstructure is build by the in-layer-solidification of low viscous photocurable resists like acrylates, urethanes or epoxies, doped with suitable photoinitiators adjusted to the used light sources (Fig 3).

At the beginning of the microstereolithography process the platform is located just below the resist's surface. An optical imaging system including a spatial light modulator like a transmission liquid crystal display or a digital micromirror device acting as a dynamic pattern generator allows the transfer of the 2D CAD-information (slice) into the polymer via solidification. The first slice data is written into the photo sensitive resist via polymerization during irradiation. After finishing, the

platform is moved a small distance towards the bottom of the reaction container and another layer can be written. The sequence can be repeated until the physical model is finished. Subsequently after part removal out of the container a post exposure curing via thermal treatment has to be performed for final polymer solidification. The microstereolithography technique developed by Bertsch [10,11] allows the fabrication of microsized parts with smallest dimensions of 5 µm. Quite recently the 2-Photon-Polymerization process enables a further miniaturization and smaller objects with structural details in the nm-range [12].

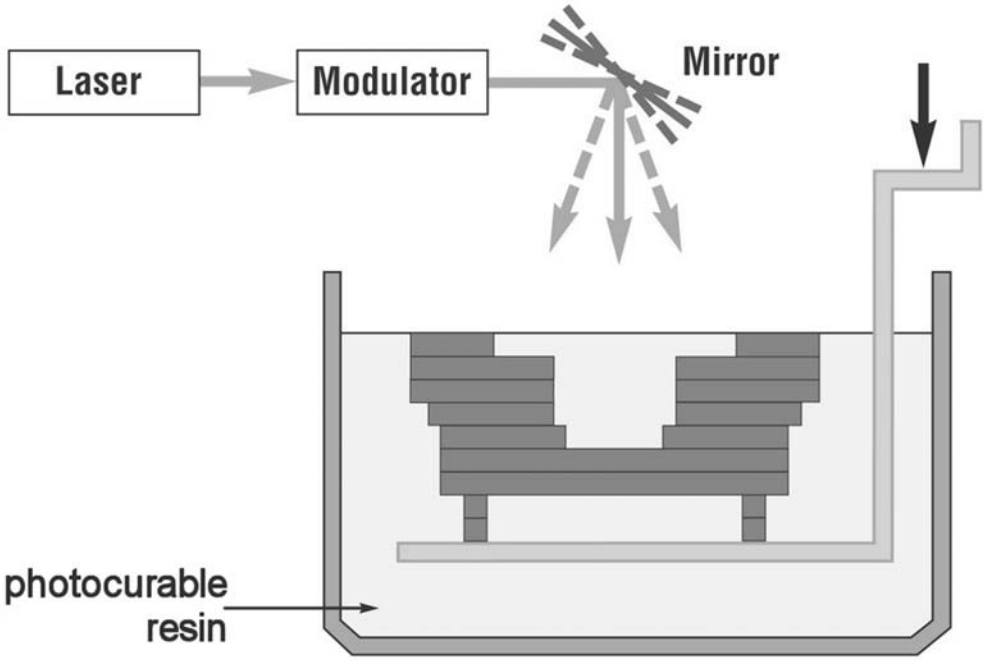


Fig. 3 Principal microstereolithography setup

3. Properties of Filler-Polymer Matrix-Composites

The addition of inorganic or organic fillers or dopants to resist materials has a strong impact on approximately all physical properties depending on the filler concentration, average particle size, particle size distribution, specific surface area, surface chemistry as well as molecular and electronic structure. If an organic dopant is soluble in the resist the resulting composite properties are mainly affected by the dopants molecular structure changing e.g. the light absorption, refractive index and important thermomechanical properties like glass transition temperature depression due to plasticizing or embrittlement a.o. Inorganic materials are insoluble in resist systems, hence the

fillers have to be dispersed in the liquid matrix, the resulting composite shows a typical multi-component, multi-phase-behaviour like light scattering and a significantly changed flow behaviour.

3.1 Flow properties

In most of the lithography variants a resist film has to be generated via spin coating or casting prior to the patterning step. The thickness and the quality of the resist film depend among other process parameters on the resist viscosity. The addition of solid inorganic or organic fillers affects the viscosity and the principal flow behaviour of polymer or resin based fluids. The viscosity is a measure for the internal friction within a fluid on a molecular level covering all interactions between individual polymer chains, solvent molecules as well as solved or dispersed particles. Following the simple approach for ideal liquids the viscosity can be described as the ratio between shear stress τ and shear rate γ (2), hence the viscosity η is constant at different shear rates (Newtonian flow behaviour). In a first approximation Newton's viscosity law can be used for almost all inorganic and organic liquids. In case of non-ideal liquids the viscosity varies with the applied shear rate, two additional fundamental flow behaviours occur. If the viscosity rises with increasing shear rate a dilatant flow can be observed. The opposite phenomenon, a viscosity drop with increasing shear rate is named pseudoplastic flow, which is typical for filled polymer resins or melts. The addition of small filler amounts show only a small impact on the resulting composite viscosity and can be described using Einstein's viscosity law originally defined for solutions and later extended for dispersions (3) [13,14]. The introduction of the relative viscosity η_{rel} (3) as quotient of the measured composite viscosity η_{comp} and the viscosity η_M of the pure liquid matrix allows a comparison of different fluid-filler-composites. The relative viscosity changes with the volume filler content Φ under consideration of a constant factor k_E , which can be estimated to a numerical value of 2.5 for small solid loads below 15vol%, neglecting particle-particle-interactions and considering monosized, non-deforming particle spheres [15]. A further power series extension of the Einstein approach introduces further parameters for geometric particle-particle interaction (k_H) (4), finally Thomas summarized a large number of experimental results in a semi empirical approach (5) for the change of the relative viscosity with filler load [16].

Newton's viscosity law $$\eta = \frac{\tau}{\dot{\gamma}} \quad (2)$$

Einstein $$\eta_{rel} = \frac{\eta_{comp}}{\eta_M} = 1 + k_E \Phi \quad (3)$$

Extended Einstein model $$\eta_{rel} = 1 + k_E \Phi + k_H \Phi^2 + \ldots \quad (4)$$

Thomas $$\eta_{rel} = 1 + 2.5\Phi + 10.05\Phi^2 + 0.00273 e^{16.6\Phi} \quad (5)$$

At low filler loads the viscosity is mainly determined by the matrix viscosity, in case of polymer based resist materials by the intermolecular polymer chain friction. At larger filler concentration filler-filler interaction occurs due to the reduced impact of the polymer fluid lubricant which results in a pronounced increase of the composite viscosity. The maximum filler load is achieved if the solid particles are in direct contact. The resulting viscosity increases to an infinite value. The observed experimental results can be described in different semi empirical approaches introducing the maximum filler load Φ_{max} in an exponential expression. The most important descriptions have been developed by Krieger and Dougherty (6) [17] and Quemada (7) [18].

Krieger-Dougherty $$\eta_{rel} = \left(1 - \frac{\Phi}{\Phi_{max}}\right)^{-k_E \Phi_{max}} \quad (6)$$

Quemada $$\eta_{rel} = \left(1 - \frac{\Phi}{\Phi_{max}}\right)^{-2} \quad (7)$$

The different models for the description of the relative viscosity change with filler load have been applied successfully in case of photocurable resist-ceramic-composites [19], thermoplastic-filler-feedstocks for injection molding [15, 20], as well as for micro- and nanofillers dispersed in UV-curable composites [21,22].

In addition to the filler content the composite's viscosity depends on the particle size distribution, the specific surface area, particle size, deformability and packing density. Table 1 shows exemplarily the properties of different micro- and nanosized aluminas. Microsized alumina powder like CT3000SG or RCHP are well established fillers for feedstock preparation used in micro injection molding. It can be depicted from Table 1 that the measured average particle sizes (d_{50}) of

the microsized aluminas differ only by a factor of 2 from the nanosized ones. The aluminas obtained from Degussa and Nanophase were described as nanosized materials with primary particle sizes of 13 and 38 nm respectively, which agglomerate to larger moieties due to surface energy minimization. The latter aluminas possess a significant larger specific surface area. The impact of the different micro- and nanosized aluminas and different filler contents on the relative viscosity of curable unsaturated polyester based composites is demonstrated in Fig. 4.

Table 1 Comparison of micro and nanosized alumina [23]

Type	**Vendor**	**Specific surface area (m^2/g)**	**d_{10} (µm)**	**d_{50} (µm)**	**d_{90} (µm)**
CT3000SG	Alcoa	7	0.071	0.266	1.002
RCHP	Baikowsky	8	0.242 (d_{20})	0.335	0.575
TM DAR	Taimei	14.5	0.104	0.165	0.297
Nanotek	Nanophase	34	0.125	0.155	0.192
C	Degussa	107	0.125	0.155	0.205

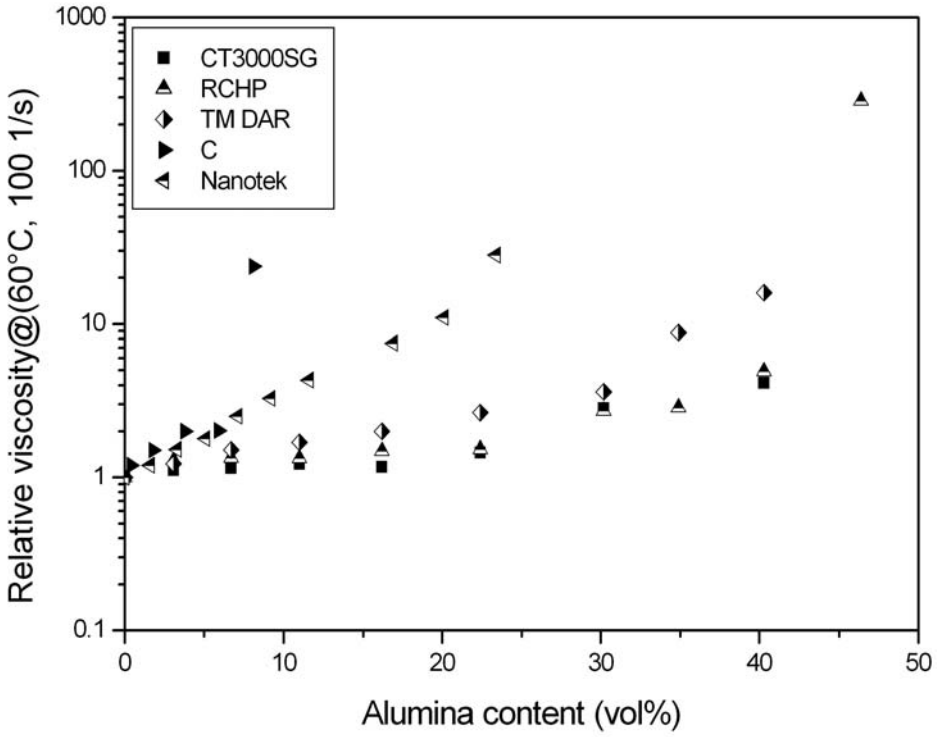


Fig. 4 Relative viscosity change of composites with filler content

As expected the increase of the specific surface results in a depression of the maximum achievable filler load, using the microsized aluminas CT3000SG and RCHP ceramic moieties more than 40 vol% can be achieved under the given experimental conditions (cone-plate-rheometer). The use of the nanosized alumina allows only small filler loads due to the large surface area, which fixes huge amounts of the liquid phase. As a conclusion the larger the filler's specific surface area the larger the resulting composite viscosity. As a consequence thin film processing like spin coating or casting of filled resists can be influenced significantly by the filler as described later in the investigated SU-8-aluminacomposites.

3.2 Optical properties

The addition of inorganic or organic fillers to polymer resist materials affects directly the optical properties. Particles with geometric extensions larger than the wavelength of light show absorption, if the average particle size is in the same range like the applied wavelength, Mie-scattering occurs. In case of smaller particles Raleigh-scattering can be observed; the intensity is proportional to $1/\lambda^4$ of the used wavelength and to the square volume of the used particles [24]. Therefore as a rule of thumb only the particles with a diameter smaller than a tenth of the used light wavelength enables an acceptable transmission.

For the realization of microstructured ceramic parts using photolithographic techniques and photocurable-ceramic-composites an estimation of the curing depth is essential. Following the modified Lambert-Beers-Law (8) the curing depth C_d is proportional to the average particle size d and the logarithm of the ratio of the incident light E_0 and the minimum intensity for photopolymerization E_c as well as indirect proportional to the filler's volume fraction Φ [25]. For highly filled composites the scattering ability can be described in terms of the scattering efficiency Q, which is a function of the refractive index difference Δn between the filler and the surrounding polymer matrix, the interparticle spacing S, a form factor F depending on the particles shape as well as the used wavelength λ (9) [25,26].

Curing depth

$$C_d = F d \frac{1}{\Phi} \frac{1}{Q} \ln \frac{E_0}{E_c} \qquad (8)$$

Scattering efficiency $$Q = (\Delta n)^2 \frac{S}{\lambda} \quad (9)$$

4. Application of filled resist systems

4.1 Nanoparticle filled resists for e-beam lithography

Nanocomposite resist systems have been developed recently containing fullerenes (C60) and silica nanoparticles based on established standard e-beam resists (ZEP520®) [27]. It was found that the incorporation of small amounts of SiO_2 nanoparticles improved the accessible resolution. Figure 5 shows line patterns with the objective of getting 40-nm structures, in the pure ZEP520®-resist a line width of 131 nm could be achieved (left image), in the composite system l47 nm lines were possible (right image). A comprehensive overview about nanolithography using organic-inorganic nanocomposites is given in [28].

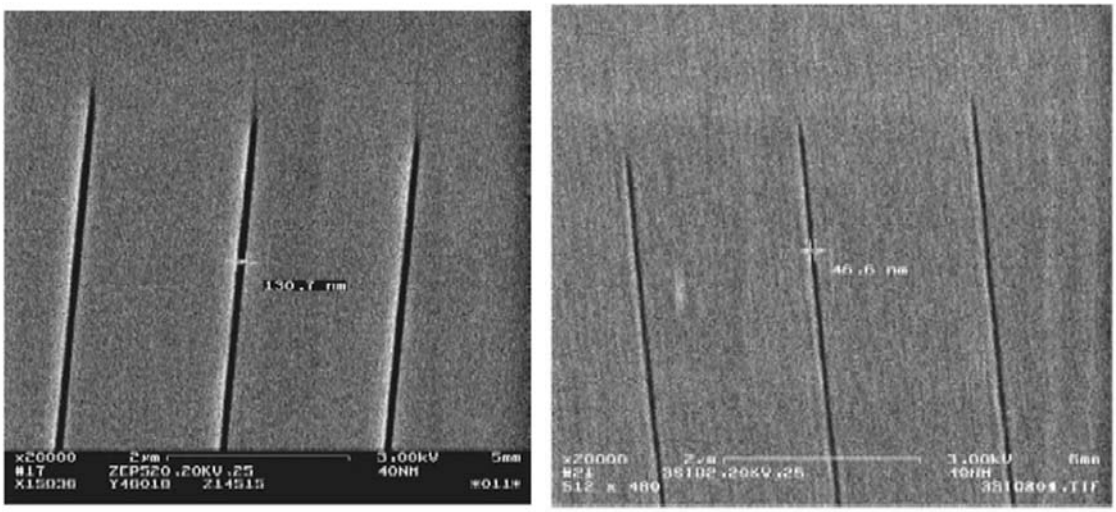


Fig. 5 SEM images of trenches after writing on pure ZEP520 (left) and ZEP-silica composite films (right) [27]

Presently the majority of e-beam resists for the realization of metallic nanostructures consist of ligand coated metal colloids, molecular organometallic species or purely inorganic materials [27-30]. In the exposed regions the material undergoes a chemical change that cleaves the stabilizing ligands from the metal cluster or atoms, respectively. The unprotected metall atoms tend

to nucleation and therefore build the metallic structure, i.e. the resists operate in negative-tone mode. Highly metallized polyferrocene-based resists allow for the fabrication of patterned metal-containing ceramics with special magnetic properties [29]. Metal salts that are soluble in organic solvents can serve as a precursor to metal atoms, if a suitable photoreactive dye is added as sensitizer. The ligand coated metal nanoparticles then act as seeds [30].

4.2 Filled preceramic polymers

Preceramic polymers are polymers, which contain in the molecular structure in addition to carbon, hydrogen, nitrogen, and oxygen silicon and sometimes boron and titanium atoms. In opposite to hydrocarbon based materials the combustion delivers ceramic residues depending on the used gas atmosphere. The pyrolysis of siloxanes (contain silicon and oxygen) under air or oxygen results silicondioxide, the firing of silazanes (contain silicon and nitrogen) under air or oxygen silicondioxide as well and under inert gas and temperatures around 1200°C to amorphous siliconcarbonitride (SICN). These materials show homogeneous elemental distribution, are free of sinter additives, and exhibit good high temperature stability and oxidation resistance [31]. The thermoplastic silazanes can be structured using X-ray lithography and subsequently be ceramized [32,33]. Several silicon containing polymers that serve as precursors for SiCN ceramic were developed in the past like the ABSE shown in Fig. 6 [31,34].

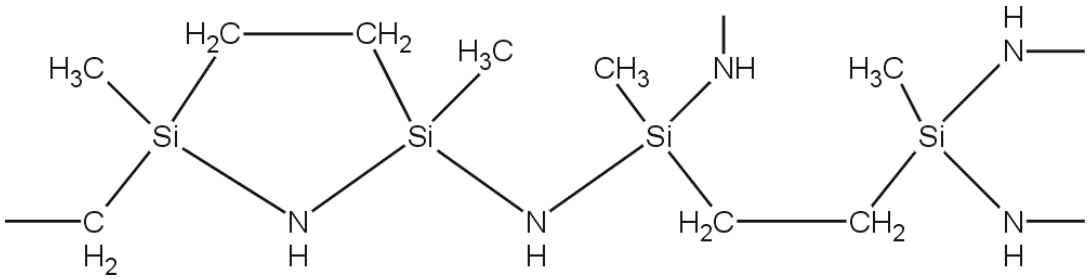


Fig. 6 Chemical structure of the preceramic polymer ABSE [34]

The selection of suitable precursors was based on the criteria listed in Tab. 2. From Tab. 3 it can be seen that none of the examined polymers fits all requirements. Several other polymers like SiBCN precursors were examined but due their improved sensitivity against moisture a use as

resist material is impossible The light sensitivity can be improved by adding suitable photo active compounds as photo initiator as in other resist materials.

Tab. 2 Required physical and chemical properties with respect to lithography [32].

a)	solid aggregate state under ambient conditions; in case of UV-lithography an adjustable highly viscous state was acceptable
b)	soluble in standard aprotic organic solvents
c)	formation of stable films on substrate surfaces
d)	processability at ambient conditions for several hours, i.e. improved chemical stability against oxygen and moisture
e)	ready and selective solubility in developing solvents
f)	high sensitivity against photo chemical induced cross linking throughout the presence of chromophoric side groups
g)	availability and small batch variation

Tab. 3 Investigated ceramic precursors and granted properties (evaluation: ++ = very good suited, - not suited) [32].

Type	Vendor	a)	b)	c)	d)	e)	f)	g)
NCP-200	Nichimen Corp.	+	+	+	+	+	+	-
SLM465012VP	Wacker	+	+	+	+	+	+	-
Ceraset	KiON Corp.	-	+	-	+	+	+	+
VL20	KiON Corp.	-	+	-	+	+	+	+
ABSE	CME Bayreuth	+	+	+	++	-	-	0

The mechanism of photo induced cross linking of a selection of these preceramic polymers was investigated using spectroscopic methods (FT-IR, NMR). It is noticeable that the exposure dose needed to measure an effect in the IR- and NMR-spectroscopy was more than 20 times higher than the dose needed for the micro structuring of the polymer using X-ray lithography. Obviously a considerably lower dose is necessary to cross link the material to an insoluble state, i.e. few linked atoms are sufficient. Absorption of the incident X-rays in the top layer causes a decrease of the deposited dose from the top to the bottom of the sample. For dose investigation the specimens were turned around after the first half of irradiation time to minimize the dose gradient and a middle dose was deposited. Figure 7 shows the dose distribution over the thickness of the specimen calculated concerning the absorption coefficient of the ABSE material [32].

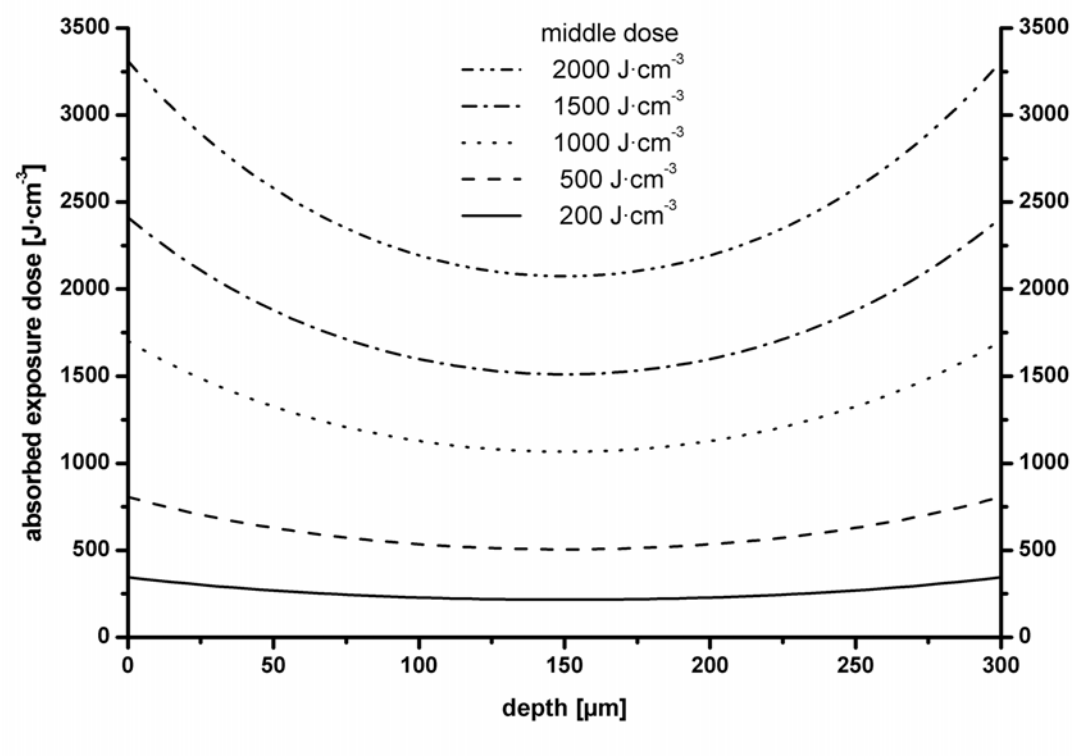


Fig. 7 Dose distribution in the X-ray irradiated ABSE samples calculated concerning the absorption behaviour [32].

Due to evaporation of volatile combustion products during pyrolysis a massive shrinkage of the samples up to 50 % occurs. This often leads to the destruction of microstructures adherent to the substrate. The idea was to minimize crack formation by mixing the polymer with 30 – 70 wt.% of a Si3N4 powder (Fa. UBE SN E10) related to the polymer content to increase the ceramic yield. Two different preceramic polymers were used in the experiments, the liquid Ceraset© and VL20 respectively and the solid ABSE precursor in a 50 wt.% solution in n-octane [32,33].
Delamination of the structures occurred during the concluding pyrolysis step because of the mismatch of the thermal expansion coefficient of the alumina substrate and the preceramic polymer film. To handle this effect, native substrates were produced from composites containing Si3N4 powder in the preceramic polymeric matrix. A tape casting process, concluded by a thermal cross linking step, was established that allows for the production of substrates with a thickness around 500 µm. Solutions of preceramic polymer as well as suspensions with different silicon nitride filler content were coated on the native substrates. After evaporation of the solvent the

samples were exposed using X-ray lithography with a micro structured test mask. The primary particles of the ceramic powder (d50 = 0.5 µm, manufacturers data) are smaller than 1/10 of the dimensions of the replicated structures. To achieve high resolution in the lithographic process it is necessary to deagglomerate the powder. A suitable deagglomeration of the □-Si3N4 powder was reached using both, an ultrasound disintegrator and a dissolving stirrer.

The silicon nitride powder absorbs the synchrotron radiation to a minor degree. The mass absorption coefficient of the elements contained in the ceramic is small, i.e. the powder in the amount used is almost transparent for the X-rays [35]. The required exposure dose for the different polymer-ceramic composites were calculated before the exposure concerning the content of Si3N4. Although the mass absorption coefficient of the Si and N atoms is low, for samples filled with powder the desired dose is rising steadily with filler content [5; 32, 35].

Samples were exposed at the ANKA synchrotron facility settled at the Research Centre Karlsruhe and the CAMD facility of the Louisiana State University, Baton Rouge. The microstructures were converted into ceramics after the patterning and development steps at temperatures up to 1500 °C. Using a bottom minimal dose of 1.5 kJ·cm^{-3} aspect ratios up to 20 were realized. The test mask layout and the resulting 3D surface topography of a sector of the exposed and developed structure based on ABSE polymer, recorded using multi layer optical microscopy is presented in Fig. 8, left side [36].

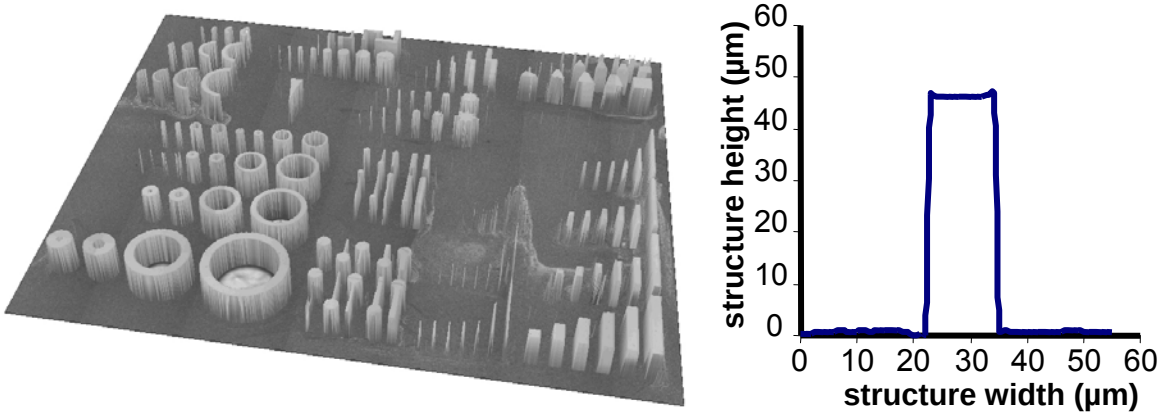


Fig. 8 Left: 3D-surface topography of a test structure mode of ABSE after deep X-ray lithography, right: height profile of a structural detail.

Structured layers with a thickness up to 200 µm have been realized [37]. The edge precision of unfilled polymer is excellent; sidewalls are perpendicular to the surface of the substrate and the pattern. The edge precision is lower than 1° as can be seen on the profile of a bar structure (Fig 8, right) from the middle of the mapped sample. At the top of Fig 9 a test structure is shown before and after pyrolysis. While the unfilled resist material except from smallest features cracked upon pyrolysis the powder filled structures remained stable (Fig 9). The surface roughness of the samples filled with powder is low compared to the side wall roughness as can be seen from the SEM pictures at the bottom of Fig 9. When the dimensions of the microstructure meet the powder particle size the quality of reproduction decreases (bottom images of Fig 9).

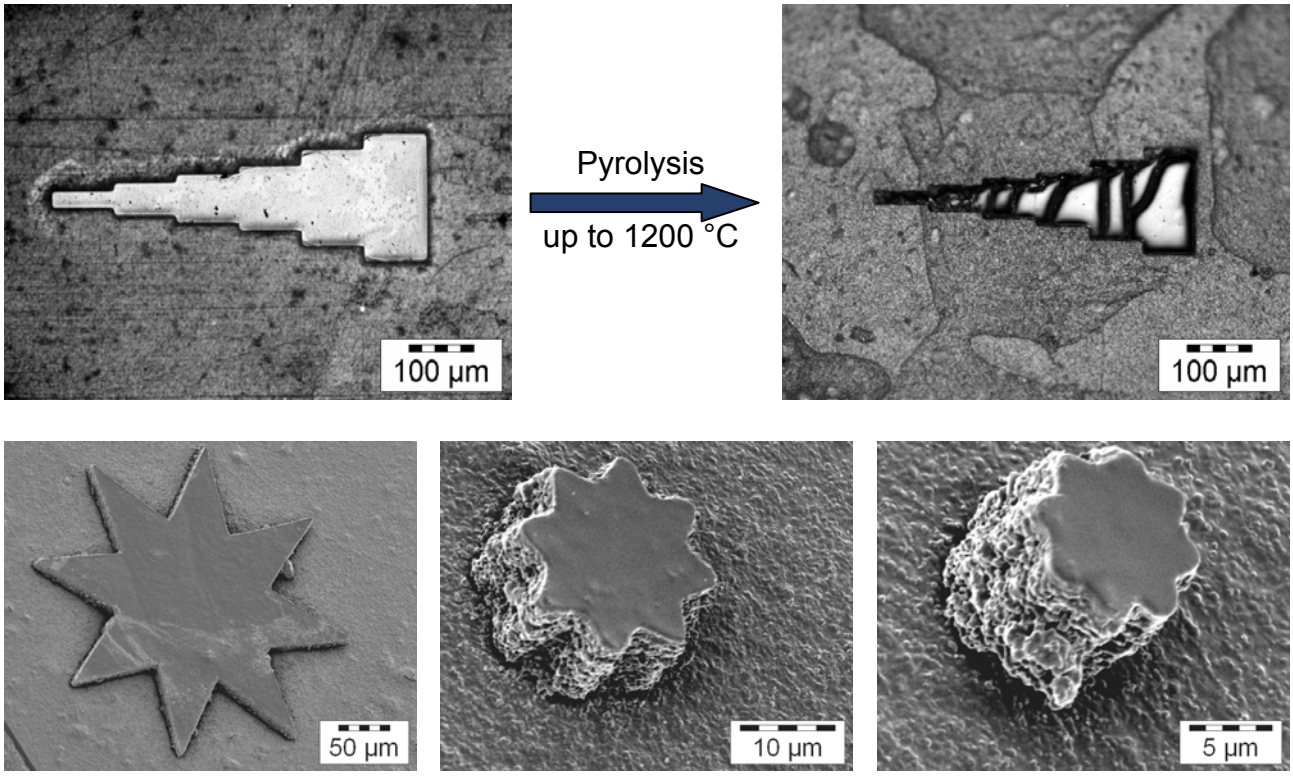


Fig. 9 Test structures made by X-ray lithography on native substrates. Top: wedge structure before and after pyrolysis of the unfilled ABSE polymer; bottom: powder filled ABSE precursor after pyrolysis

Using deep X-ray lithography a value for the contrast of the unfilled ABSE material was calculated. The contrast describes the sensitivity of a resist material in X-ray lithography. Following (10) for the

ABSE material a contrast value around 0.8 was determined. D_0 is the dose without any effect on the resist, D_{100} the related value for a complete solidification. With a sensitivity against crosslinking by synchrotron radiation of 500 – 1000 J/cm^3 the preceramic polymer ABSE as a negative resist ranges between the values of the standard resist materials SU-8 (15 J/cm^3, negative resist) and PMMA (4000 J/cm^3, positive resist).

Contrast $$\gamma = \frac{1}{\log \frac{D_{100}}{D_0}} \qquad (10)$$

Influence of Suspension Composition and Treatment

The treatment of the suspensions is of great influence on porosity; density and hardness of the resulting fired ceramic. The extended deagglomeration by ultrasonic treatment caused a significant decrease in the porosity (Fig. 10). The influence of the aggregation on the substrate quality can also be seen from the Vickers hardness. Maximum hardness of 1068 ± 36 HV was achieved at 50 wt.% (24.5 vol.%) for ultrasound treated samples (SSN HV10 = 1400).

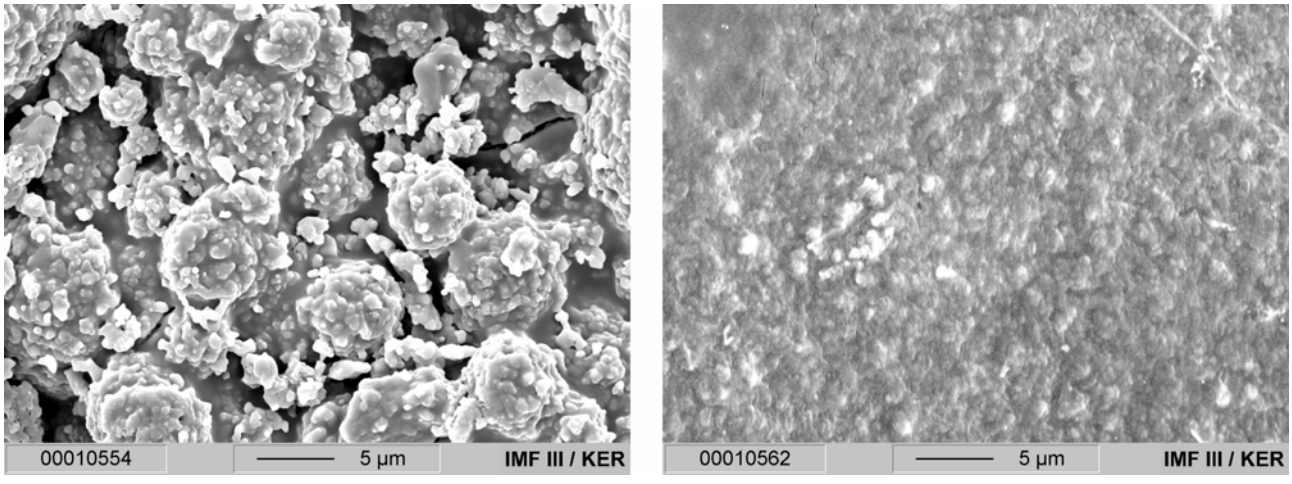


Fig. 10 Tape casting suspensions treated without (left) and with ultrasound (right). SEM pictures of the pyrolysed substrates.

Admittedly for the pyrolytic conversion into the amorphous SiCN ceramic, film thickness should be limited as crack formation is deteriorating with increasing dimensions especially for unfilled preceramic resist materials.

4.3 Filled SU-8 resists

The main purpose of adding fillers to SU-8 is the exploitation of the outstanding sensitivity against UV- and x-ray radiation. Different approaches for the introduction of electrical or magnetic properties for the realization of composite microcomponents have been described in literature. In a quite different approach SU-8-alumina composites can be microstructured via deep x-ray lithography. After thermal post processing ceramic microcomponents can be obtained.

4.3.1 Electrical conductive SU-8-composites

SU-8-based composites containing up to 40 vol% microsized silver particles (average diameter around 1.5 µm) show electrical conductivity [38]. As in other described resist-filler systems (see section 4.4) the curing depth decreases with increasing silver content. At filler contents larger than the electrical percolation threshold of 6 vol% the polymerized layers have a thickness of less than 20 µm. Using the UV-LIGA technique simple test structures (thickness 8 µm) for resolution tests (Fig. 11, left) or even wheel structures (Fig. 11, right) can be realized [38,39].

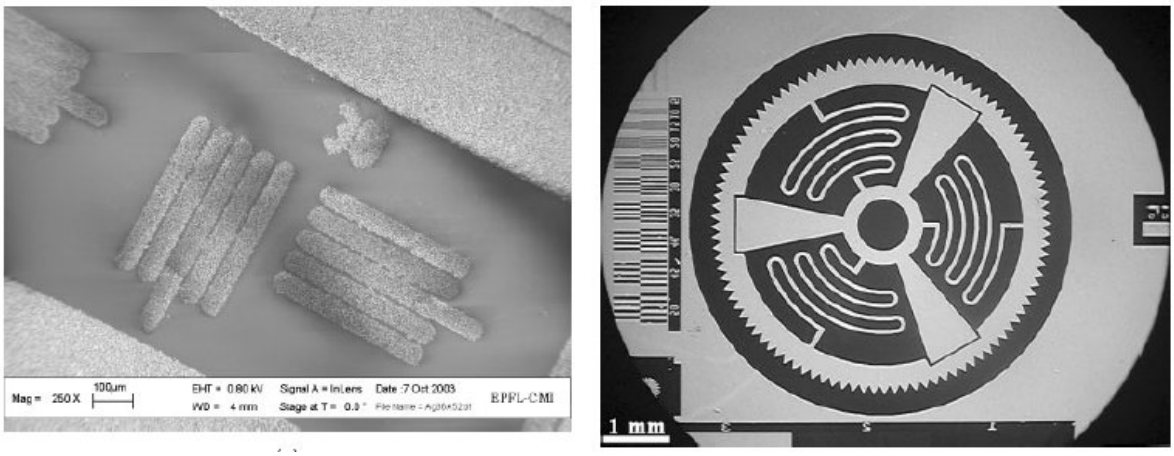


Fig. 11 Images of SU-8-silver test structure (left) and wheel (right) [38].

4.3.2 Magnetic SU-8-composites

Ferromagnetic resists can be realized by incorporating micro- or nanosized ferromagnetic materials like nickel or BaFe [40,41]. The addition of nanosized nickel powder (average particle size 80-150 nm) decreased even at very low loads of 4 wt%% the optical transmission properties. Due to scattering, reflection and diffraction of light a patterning via UV lithography was successful using the 365 and 405 nm wavelengths at thin films with a thickness around 70 µm. The magnetic resist was further used for the fabrication of cantilevers as micromirror substrates.

4.3.3 Silica filled SU-8 for microelectronic applications

The addition of transparent silica microsized particles to SU-8 improves the thermal stability up to 360°C and adjusts the coefficient of thermal expansion (CTE) to common solder material [42]. The filled resist can be used as solder mask during circuit fabrication. The filler content can be varied between 30 - 70 wt% with respect to the targeted CTE. Depending on the filler content the filled SU-8 can be photocured with a dose around 0.05 - 0.4 J/cm² in the UV.

4.3.4 Lithographically-anchored nanoparticle synthesis (LANS)

Iron nanoparticles can be fabricated by electron beam lithography of a calix[6]arene based negative resist doped with the iron complex $Fe(AcAc)_3$ [43]. The exposure to the e-beam and subsequent thermal treatment forms iron nanoparticles only at the positions were the original resist pattern had been generated. The metal nanoparticles with an average height of 1.7 nm can be used as catalyst for the growth of carbon nanotubes via ethanol CVD in an evacuated quartz tube.

4.3.5 SU-8-alumina-composites

For the realization of ceramic microcomponents fabricated using deep x-ray lithography, a similar process sequence as described in section 4.2 had to been applied using SU-8 as photoresist due to the outstanding crosslinking behavior filled with two different submicron aluminas (Alcoa CT3000SG and Reynolds RC-HP w/o Mg, properties see Table 1). The process comprises the individual process steps composite formation, film processing, deep x-ray lithography and thermal post treatment like debinding and sintering to the final alumina part [35].

Composite formation and film processing

The addition of ceramic fillers to reactive resins or resists yields in general to a moderate increase in the flow behavior at low filler load. Entering the critical region around 40 vol% solid content, the viscosity increases dramatically over several decades. For the realization of ceramic microcomponents, a ceramic filler content of the composite should be around 45-50 vol% in order to avoid an enhanced part warpage or anisotropic shrinkage effects. To evalutate the flow behaviour of SU8-alumina composites the change of the relative viscosity with alumina load was investigated (Figure 12). The dependence of the relative viscosity with filler load is quite similar as described in section 3 and shown in Figure 4. At low filler loads up to 30vol% a moderate viscosity increase can be observed at both presented shear rates, a further alumina addition up to 42vol% yield a relative viscosity increase by a factor 20 lat the low shear rate of 10 1/s. The increase of the relative viscosity with alumina load follows the Quemada approximation as described in section 3.1. The large composite viscosity prevents the use of spin coating as film formation method; therefore a modified casting technique was developed as described in [35]. Different layer thicknesses up to 500 µm could be realized; the subsequent soft-baking step had to be adjusted to the individual layer thicknesses.

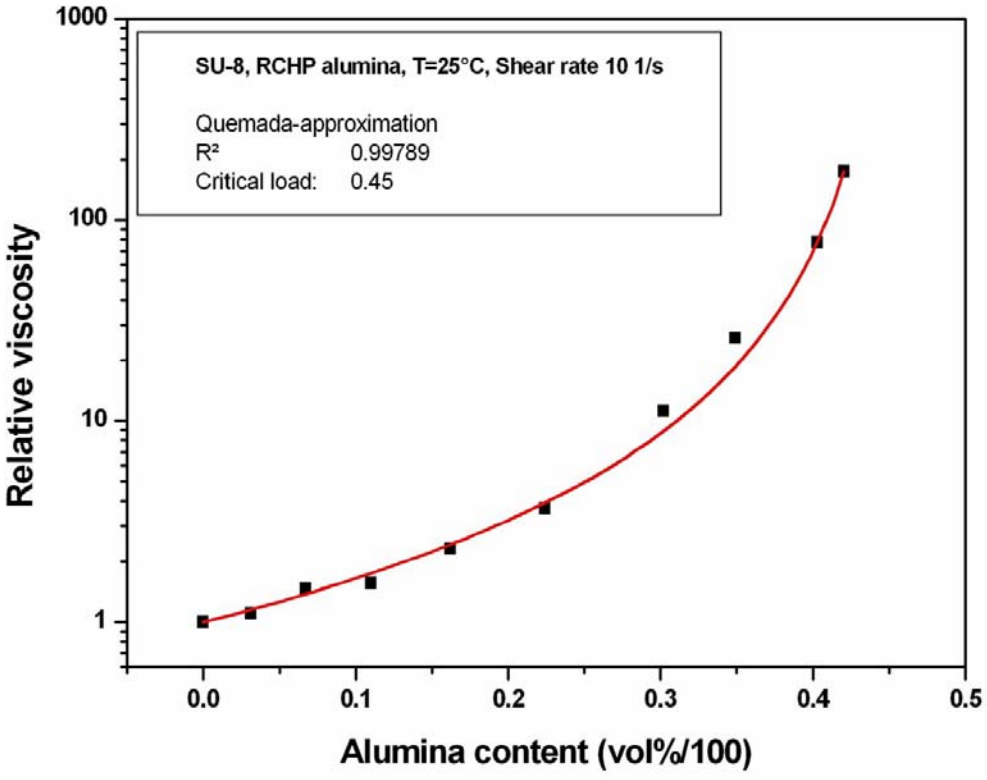


Fig. 12 Relative viscosity change of the SU-8-RCHP alumina composite with filler load

Deep x-ray lithography

Beryllium mask membranes deliver the best contrast due to the low atomic number of the material. IAs the aluminum oxide powder does increase the absorption of the x-rays in the resist, the minimum dose was expected to be considerably higher than the bottom dose used for pure SU-8 resist of 15 J/cm^3. A dose screening yielded an imperative bottom dose of 400 J/cm^3 for a full resist crosslinking. The fluidic microstructures shown in Figure 13 are 20 µm wide and about 200 µm deep with an aspect ratio of 10. At the right side of Figure 13 a circular inlet and the channel opening are magnified showing the improved smoothness of the layer surface and channel walls. The reduced sidewall surface roughness is caused by the alumina particles at the boundary between exposed and unexposed areas [35].

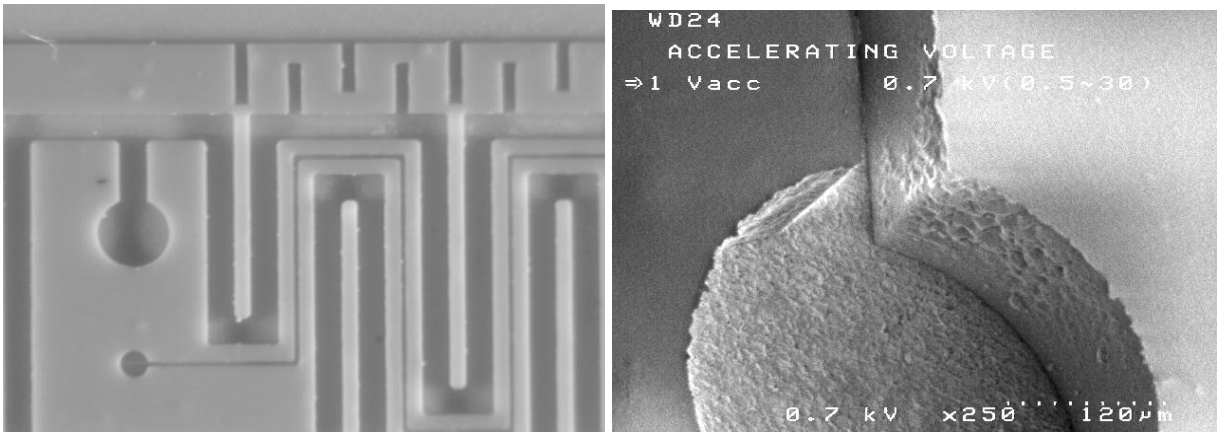


Fig. 13 Microscopic and SEM-images of microfluidics structures after development [35]

Thermal postprocessing

Thermogravimetric investigations on the pure SU-8 yielded the decomposition behaviour at elevated temperatures up to 600°C which is important for the crack free realization of the pure alumina microcomponents. After debinding the final sintering step at 1550°C followed. Figure 14 shows exemplarily free standing high aspect ratio test structures after debinding, Figure 15 the same microstructures after sintering. Prior to debinding the posts have an average height of 360 µm and a diameter of 40 µm, the small walls a length of 100 µm, a thickness of 10 µm and a height of 160 µm gaining an aspect ratio of 16. Especially in the sintered structures agglomerates of the ceramic particles are visible on the sidewalls.

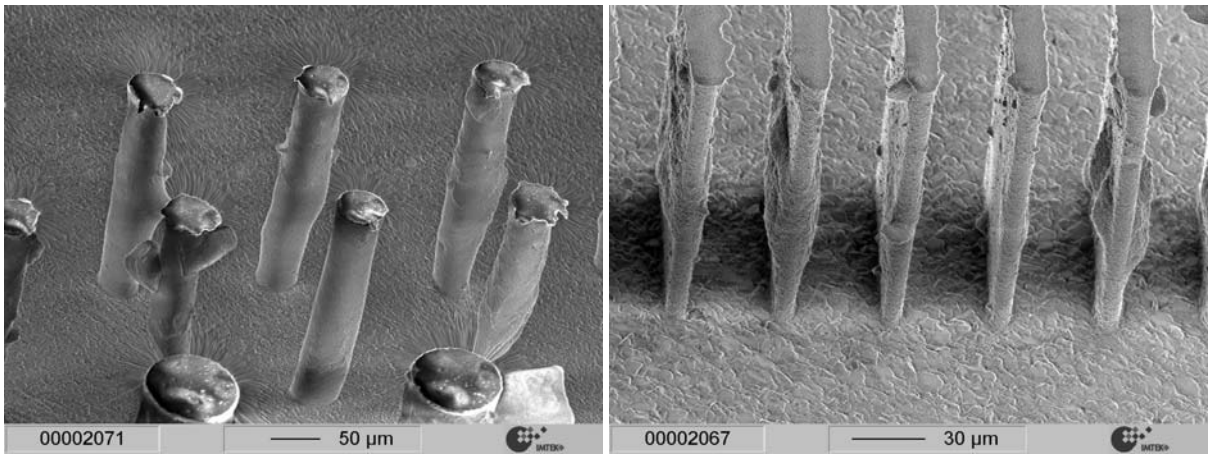


Fig. 14 Free standing high aspect ratio posts and walls before thermal treatment [35]

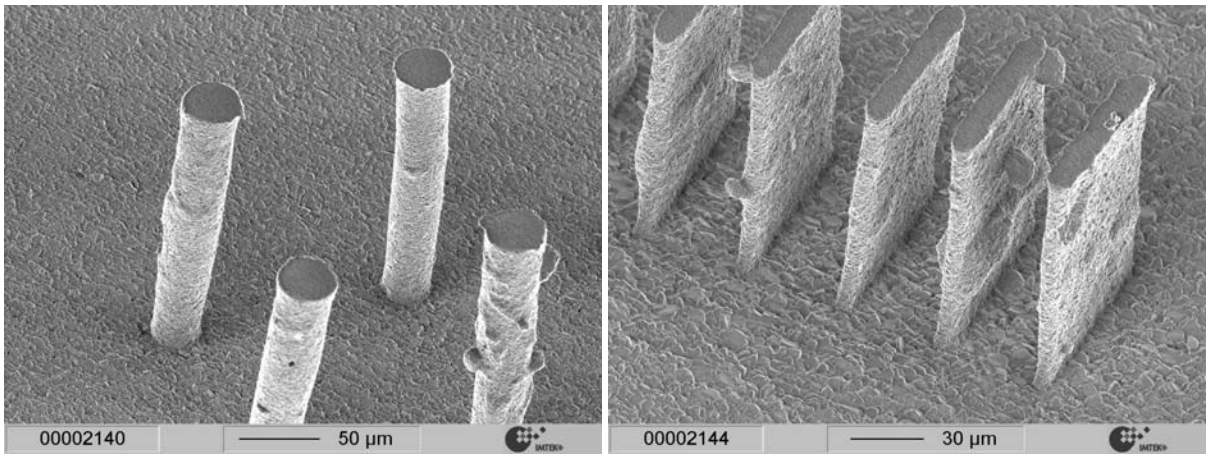


Fig. 16 Free standing high aspect ratio posts and walls after thermal treatment [35]

4.4 Filled resists for microstereolithography

Resins or resist system for microstereolithography must fulfil the following basic requirements [44]:

- low viscosity for a better resist flow and layer thickness control
- large curing speed
- isotropic polymerization
- good structural accuracy
- by composition adjustable and advantageous mechanical properties.

Since the last 10 years a large number of papers dealing with different variants of microstereo-lithography applied to filled resist systems, in most of the cases alumina or PZT. Griffith and Halloran extended the established stereolithography process to the fabrication of ceramics by adding silica, alumina or silicon nitride to photocurable aqueous acrylamide and non-aqueous diacrylate resists [25]. As described in section 3.2 the curing depth is amongst others a function of

the filler type, the filler's refractive index, the particle size and the load in the resist. The latter one affects directly the resists viscosity, for the used commercial equipment (SLA-250, 3D Systems) the composite's viscosity must be lower than 3 Pa s, which was achieved at an alumina load of 40 vol% in the diacrylate system.

In case of a silica load of 50vol% in different aqueous UV-curable systems curing depths between 250 and 700 μm could be achieved with a dose of 1.5 J/cm², which is more than three times larger than for the pure resists. The curing behaviour at larger loads is dominated by scattering effects. With increasing solid load the curing depth is reduced. The particle size affects the cure depth significantly, in case of different alumina an average particle size reduction from 0.61 to 0.34 μm yielded a cure depth increase from 300 to 450 μm. Using a SLA-250 stereolithography apparatus and composites based on the diacrylate system simple windowpane test structures or curved line profiles could be solidified to green bodies, which could be transferred into solid dense alumina by sintering at 1550°C [25,45].

The first ceramic microcomponents, namely alumina microgears with diameters of 400 and 1000 μm (thickness 20 μm), were fabricated from aqueous and non-aqueous alumina filled resists with a solid load of 33 vol% using a microstereolithography apparatus and subsequent debinding and sintering [46]. The achieved density was only 56% of the theoretical value of 3.9 g/cm³.

A similar approach using a highly viscous photocurable ceramic paste instead of a low viscous resin as in stereolithography was described by Doreau [47]. The modified process allowed resists with a ceramic load up to 65 vol%. A further process improvement allowed the fabrication of microstructured alumina parts with a density of 97% of the theoretical value (Fig. 18). The best dimensional resolution is around 230 μm with an used irradiation dose (laser beam irradiation, λ = 351-364 nm) of 0.05 J/cm² [48] in an acrylate based resist. PZT-transducer elements have been fabricated by stereolithography as first active microcomponent using an acrylate resist filled with microsized PZT-filler [19]. The density of the ceramic was around 94% after firing.

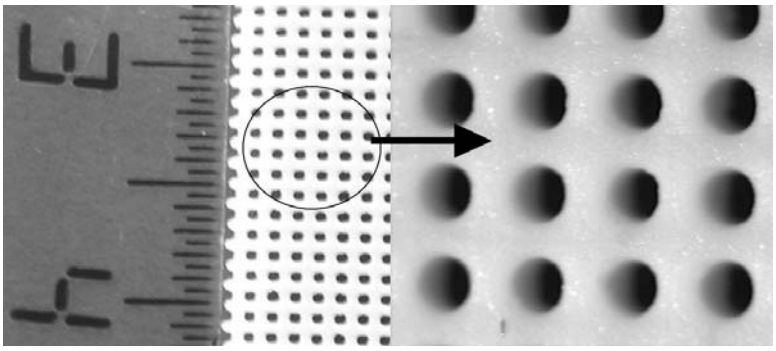


Fig. 16 Sintered alumina mesh pattern (hole diameter: 600 µm, pitch: 230 µm, layer thickness 25 µm) (permission missing, [48]).

The realization of smaller structural details and a reduced layer thickness requires finer ceramic particles in the submicron range. As described earlier, the addition of nanofillers instead of microsized fillers result in a significant increase of the composite viscosity due to the large specific surface area. The best compromise is a ceramic with a low specific surface area and a submicron average particle size. As an typical example Bertsch and coworkers used an alumina filler with an average particle size of 300 nm and a specific surface area around 9 m²/g, dispersed in an polyethylenglycole 400 diacrylate [49,50]. The viscosity of the used composite systems increased significantly with increasing filler content up to values of 50 Pa s at low shear rates. Three dimensional microcomponents like a teapot structure (Fig 17, left) consisting of 295 layers with an individual thickness of 10 µm or a screw can be fabricated within 90 minutes. After firing the final ceramic microcomponent with a shrinkage around 20% can be obtained (Fig 17, right).

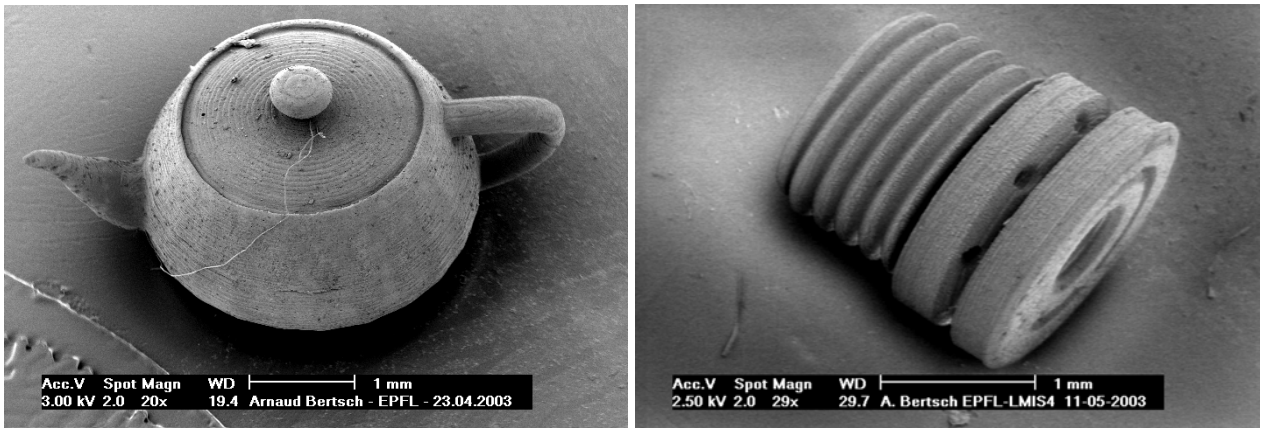


Fig. 17 Left: Resist-alumina composite teapot; right sintered alumina screw [49], with permission from IOP Publisher Limited

Tape casting

Quire similar requirements as in microstereolithography are valid for UV curable composites used in tape casting. Chartier et al [51] reported about the development of composites consisting either of alumina or zirconiumdioxide with an average particle size around 0.6 µm, dispersed in hydroxyethyl methacrylate using Darocur 1173 from Ciba as photoinitiator. The dispersion was cured using a wide band emission UV lamp (200 – 450 nm). The authors investigated systematically the influence of the incident light energy, the photoinitiator concentration, the exposure conditions, the difference of the resists and filler refractive index, the filler volume fraction on the curing behaviour and the resulting penetration depth in the composite film as described in section 3.2 [Char1999]. The following basic correlations were found:

- an increase of the irradiation energy results an increase of the curing depth
- for each composite an optimized photoinitiator concentration exists
- the curing depth decreases with increasing filler volume fraction due to scattering.

Sheets of alumina (30 vol%) filled methacrylate with a thickness up to 700 µm have been photocured after tape casting.

Metal filled resists

Resist systems filled with metal powders have been described for the first time quite recently [52]. Lee and coauthors used fine copper powder (average particle size around 3 µm), dispersed in a photocurable mixture of 1,6-hexanediol-diacrylate (HDDA), trimethylol propane triacrylate (TMPTA), N-vinyl-pyrrolidone (NVP) as diluent and dimethoxy-phenyl-acetophenone (DMPA) as photoinitiator and a dispersant for improved laser light penetration producing a scattering effect [Lee2006]. The resulting composite containing 60 wt% metal filler shows a viscosity of 100 mPa s at 26°C and can be photocured using either a UV lamp (290 - 450 nm) or an Ar ion laser (351.1 nm) integrated in a microstereolithography system. As first simple examples a microtube (Fig. 18, left side) with an inner diameter of 320 µm was generated by 20 curing steps of each 50 µm layer thickness. The helical gear (Fig. 18, right side) was fabricated by a rotation of 3° between

each layer formation and consists of 30 layers with an individual height of 50 µm. The resulting total height is 15550 µm. The final copper microcomponents were obtained by debinding and vacuum sintering (Fig. 19). Unfortunately the authors gave no information about the resulting sinter density.

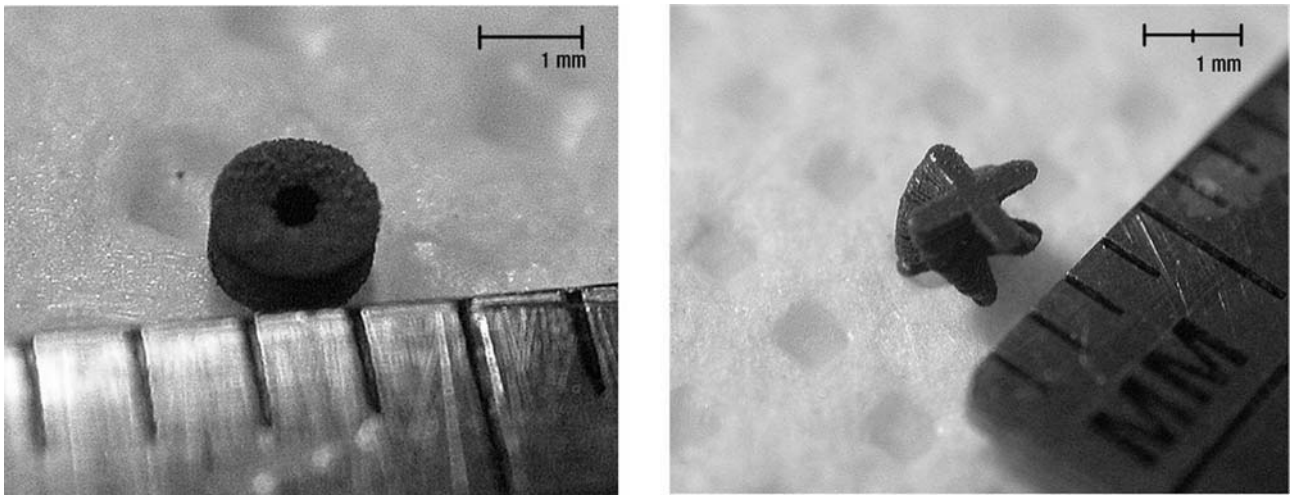


Fig. 18 Images of small photopolymer-copper components [52], with permission from Elsevier.

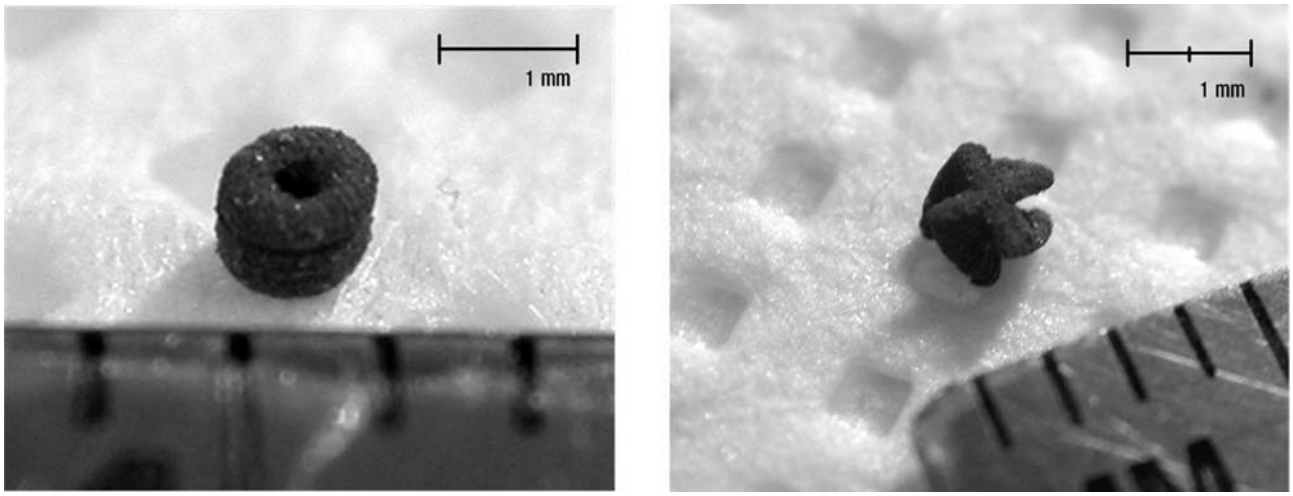


Fig. 19 Images of small copper components after sintering [52], with permission from Elsevier.

5 Miscellaneous

5.1 Photosensitive polyimide/silica composites

Photosensitive polyimides are widely use in microelectronics like packaging or in printed circuit boards [53]. The large volume shrinkage up to 50% hinders the use of this polymer class in MEMS or in optoelectronic devices as resist material due to a pronounced distortion of the resulting

pattern like rounded edges a.o. Wang and coauthors describe the synthesis of a novel ionic-salt type photopatternable fluorinated polyimide/silica hybrid material with improved physical properties. Thin films of different polyimide/silica compositions were prepared via spin coating, then cured by UV light at 365 nm with a dose of 1.8 J/cm² using a chromium mask and finally post-exposure-baked at 90°C. After developing in a mixture of γ-butyrolactone/DMSO/water the final pattern was imidized at temperatures up to 300°C. The finally obtained polyimide show glass transition temperatures up to 280°C, a reduced coefficient of thermal expansion and good optical transmission properties in the NIR-range (1319 nm). Increasing silica amounts reduce the index of refraction. Figure 20 shows examples of waveguides prepared by photolithography. The used composites have potential for the use as optical waveguides prepared by UV lithography.

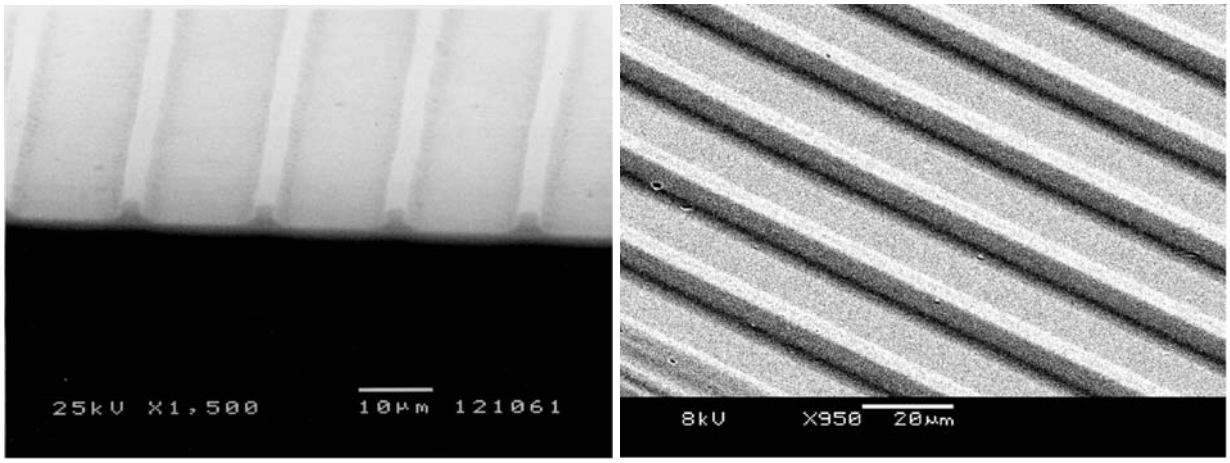


Fig. 20 SEM images of developed patterns using different polyimide/silica compositions [53], with permission from Elsevier.

5.2 Water based filled photoresists

Water based photopolymerisable epoxy resist formulations can be filled with organic or inorganic fillers like polyvinylacetate-polyvinylchloride copolymers, starch, silica, kaolin or titanium dioxide for an improvement of the dried film quality after coating [54]. A similar approach using an ethylenically unsaturated dextrin oligomer, doped with large surface inorganics like silica for an improved scratch resistance and wet strength [55]. During patterning using UV sources the resist behaves as a negative resist and gets water insoluble. Both systems are designed for the realization of lithographic printing plates.

5.3 Three dimensional lithography using sol-gel based compositions

Organic-Inorganic hybrid polymers like ORMOCER®s carrying light sensitive organic moieties like acrylates, styryl, or epoxy units can be patterned in standard photolithography [56]. Real 3D-nanostructures like photonic crystals can be generated in a two-photon-absorption process by using femtosecond laser pulses.

6 Summary

Filled resists systems containig mainly inorganic materials are widely used in approximately all established variants of 2.5D lithography starting with EBL and ending with the generation of real 3D microcomponents via microstereolithography. The addition of fillers is motivated by such different aspects like film stabilization, resolution enhancement, controlled synthesis of carbon nanotubes as well as the direct realization of ceramic and metal components via lithography avoiding intermediary molding steps. A successful use of filled resists depends strongly on the adaption of the standard resist technology to the physical properties of the composite resist systems, especially the flow behaviour with the significantly larger viscosity, which affects directly the film formation, and the reduced curing depth during irradiation due to scattering and absorption.

7 Acknowledgement

The authors thank J. Goettert (LSU-CAMD), M. Boerner (FZKa-ANKA) and G. Motz (Univ. Bayreuth) for their continous support during our common research in the last years.

8 References

[1] R. W. Peiffer, Application of Photopolymer Technology, in: Photopolymerization - Fundamentals and Applications, A.B. Scranton, C.N. Bowman, R.W. Peiffer (eds.), *ACS Symposium Series* **1997**, *Vol. 673*, 1-14.

[2] H. Ito, E. Reichmanis, O. Nalamasu, T. Ueno, Micro- and Nanopatterning Polymers, *ACS Symposium Series* **1999**, Vol. 706.

[3] W. Menz, J. Mohr, O. Paul, *Microsystem Technology*, Wiley-VCH, Weinheim, FRG, **2001**.

[4] S. A. Campbell, The science and engineering of microelectronic fabrication. Oxford Univ. Press, New York, USA, **1996**.

[5] P. Meyer, J. Schulz, L. Hahn, DoseSim: Microsoft-windows graphical user interface for using synchrotron x-ray exposure and subsequent development in the LIGA process, *Review of Scientific Instruments,* **2003**, 74, *2,* 1113.

[6] T. Hanemann, W. Bauer, R. Knitter, P. Woias, Rapid prototyping and rapid tooling techniques for the manufacturing of silicon, polymer, metal and ceramic microdevices, in: *MEMS/NEMS Handbook: Techniques and Applications*, Ed: C. T. Leondes, Springer Publisher, Berlin, FRG, **2006**, pp187-255, ISBN: 0-387-24520-0.

[7] T. Takagi, N. Nakajima, Architecture combination by micro photoforming process, **1994**, *IEEE Proc. Micro Electro Mechanical Systems MEMS´94*, 25.-28.01.1994, Oiso, Japan, pp211-216.

[8] K. Ikuta, K. Hirowatari, T. Ogata, Three dimensional micro integrated fluid systems (MIFS) fabricated by stereo lithography, **1994**, *IEEE Proc. Micro Electro Mechanical Systems MEMS'94*, 25.-28.01.1994, Oiso, Japan, pp 1-6.

[9] C. H. Hull, Apparatus for production of 3D objects by stereolithography, 3D Systems **1984**, US Pat. 4,575,330

[10] A. Bertsch, S. Zissi, J. Y. Jezequel, S. Corbel, J. C. Andre, Microstereolithography using a liquid crystal display as dynamic mask-generator", *Microsyst. Techn.* **1997**, *3(2)*, 42-47.

[11] A. Bertsch, H. Lorenz, P. Renaud, 3D microfabrication by combining microstereolithography and thick resist UV lithography, *Sensors and Actuators* **1999**, *73*, 14-23.

[12] M. Straub, L. H. Ngyuen, A. Fazlic, M. Gu, Complex-shaped three-dimensional microstructures and photonic crystals generated in a polysiloxane polymer by two-photon stereolithography", *Optical Materials* **2004**, *27(3)*, 359-364.

[13] A. Einstein, Eine neue Bestimmung der Moleküldimension, *Ann. Physik* **1906**, *19*, 289-306.

[14] A. Einstein, Berichtigung zu meiner Arbeit: Eine neue Bestimmung der Moleküldimension, *Ann. Physik* **1911**, *34*, 591-592.

[15] R. G. German, Powder Injection Molding **1990**, Metal Powder Industries Federation, Princeton, New Jersey, USA.

[16] D. G. Thomas, Transport characteristics of suspension: VIII. A note on the viscosíty of newtonian suspensions of uniform spherical particles, *J. Colloid Sci.* **1965**, *20*, 267-277.

[17] I. M. Krieger, T. J. Dougherty, A mechanism for non-newtonian flow in suspensions of rigid spheres", *Trans. of the Soc. Rheology* **1959**, *III*, 137-152.

[18] D. Quemada, Rheology of concentrated disperse systems and minimum energy dissipation principle - I. Viscosity-concentration relationship, *Rheol. Acta* **1977**, *16*, 82-94..

[19] O. Dufaud, P. Marchall, S: Corbel, Rheological properties of PZT suspensions for stereolithography, *Journal of the European Ceramic Society* **2002**, *22*, 2081-2092.

[20] I. Agote, A. Odriozola, M. Gutierrez, A. Santamaria, J. Quintanilla, P. Coupelle, J. Soares, Rheological study of waste porcelain feedstocks for injection molding, *J. Europ. Ceram. Soc.* **2001**, *21*, 2843-2853.

[21] T. Hanemann, Influence of dispersants on the flow behaviour of unsaturated polyester-alumina-composites, *Composites A: Applied Science and Manufacturing* **2006**, *37(5)*, 735-741.

[22] T. Hanemann, R. Heldele, J. Hausselt, Particle size dependent viscosity of polymer-silica-composites, *Proc. 4M 2006 - 2nd International Conference on Multi-Material-Micro-Manufacture (4M)*, 20.-22.09.**2006**, Grenoble, Frankreich.

[23] T. Hanemann, K. Honnef, J. Haußelt, Rapid Prototyping of Ceramic Microcomponents Using Nanosized Alumina, *Nanofair 2004-New Ideas for Industry* **2004**, VDI-Berichte, 1839, 175-178, ISBN 3-18-091839-X.

[24] P. Ajayan, L. Schadler, P. Braun, Nanocomposite Science and Technology, **2003**, Wiley-VCH, Weinheim, FRG, p140.

[25] M. L. Griffith, J. W. Halloran, Freeform Fabrication of Ceramics via Stereolithography, *J. Am. Ceram. Soc.* **1996**, *79(10)*, 2601-2608.

[26] T. Chartiers, C. Hinczewski, S. Corbel, UV curable systems for tape casting, *Journal of the European Ceramic Society* **1999**, *19*, 67-74.

[27] L. Merhari, K.E. Gonsalves, Y: Hu, W. He, W.-S. Huang, M. Angelopoulus, W.H. Bruenger, C. Dzionk, M. Torkler, Nanocomposite resist systems for next generation lithography, *Microelectronic Engineering* **2002**, *63*, 391-403.

[28] K. E. Gonsalves, L. Merhari, H. P. Wu and Y. Q. Hu, Organic-inorganic nanocomposites: Unique resists for nanolithography, *Advanced Materials,* **2001**, 13, *10,* 703-714.

[29] S. B. Clendenning, S. Aouba, M.S. Rayat, D. Grozea, J.B. Sorge, P.M. Brodersen, R.N.S. Sodhi, Z.-H. Lu, C.M. Yip, M.R. Freeman, H.E. Ruda, I. Manners, Direct writing of patterned ceramics using electron-beam lithography and metallopolymer resists, *Advanced Materials* **2004**, *16(3)*, 215 - 219.

[30] F. Stellacci, C. A. Bauer, T. Meyer-Friedrichsen, W. Wenseleers, V. Alain, S. M. Kuebler, S. J. K. Pond, Y. D. Zhang, S. R. Marder and J. W. Perry, Laser and electron-beam induced growth of nanoparticles for 2D and 3D metal patterning, *Advanced Materials,* **2002**, *14(3),* 194-198.

[31] E. Kroke, Y. L. Li, C. Konetschny, E. Lecomte, C. Fasel and R. Riedel, Silazane derived ceramics and related materials, *Materials Science & Engineering R-Reports,* **2000**, 26, *4-6,* 97-199.

[32] M. Schulz, M. Boerner, J. Hausselt, R. Heldele, Polymer derived ceramic microparts from x-ray lithography: cross-linking behavior and process optimization, *Journal of the European Ceramic Society* **2004**, *25(2-3)*, 199-204.

[33] M. Schulz, J. Hausselt and R. Heldele Structuring Ceramics Using Lithography. 29th International Conference on Advanced Ceramics and Composites, Symposium on Mechanical Behavior and Design of Engineering Ceramics and Composites, Cocoa Beach, Florida, American Ceramic Soc., Westerville, Ohio, **2005b**.

[34] G. Motz, J. Hacker and G. Ziegler, Special Modified Silazanes for Coatings, Fibers, and CMCs, *Ceramic Engineering and Science Proceedings,* **2000**, 4, *21*.

[35] C. Mueller, T. Hanemann, G. Wiche, C. Kumar and J. Goettert, Fabrication of ceramic microcomponents using deep X-ray lithography, *Microsystem Technologies* **2005**, *11(4-5),* 271-277.

[36] M. Schulz, M. Börner, J. Göttert, T. Hanemann, J. Hausselt and G. Motz, Cross linking behavior of preceramic polymers effected by UV- and synchrotron radiation, *Advanced Engineering MaterialS,* **2004**, *6(8),* 676-680.

[37] T. Hanemann, M. Ade, M. Borner, G. Motz, M. Schulz and J. Hausselt, Microstructuring of preceramic polymers, *Advanced Engineering Materials,* **2002**, *4(11),* 869-873.

[38] S. Jiguet, A. Bertsch, H. Hofmann, P. Renaud, SU8-Silver photosensitive nanocomposite, *Advanced Engineering Materials* **2004**, *6(9)*, 719 - 724.

[39] S. Jiguet, M. Judelewicz, s. Mischler, A. Bertsch, P. Renaud, Effect of filler behavior on nanocomposite SU8 photoresist for moving micro-parts, *Microelectronic Engineering* **2006**, *83(4-9)*, 1273-1276.

[40] N. Damean, B.A. Parviz, J. N. Lee, T. Odom, G.M. Whitesides, Composite ferromagnetic photoresist for the fabrication of microelectromechanical systems, *J. Micromech. Microeng.* **2005**, *15*, 29-34.

[41] M. Bedenbecker, H. H. Gatzen, Herstellung polymergebundener Hartmagnete durch in SU-8 eingebrachtes Magnetpulver, Proc. MST-Kongress 2005, 10.-12.10.2005, Freiburg, FRG, **2005**.

[42] V. R. Markovich, A. A. Mehta, E. R. Skarvinko, D. W. Wang, Thermally stable photoimaging composition, *EP 480154*, **1991**.
[43] M. Ishida, H. Hongo, F. Nihey, Y. Ochiai, Diameter-controlled carbon nanotubes grown from lithographically defined nanoparticles, *Japanese Journal of Applied Physics* **2004**, *43(10B)*, L1356-L1358.
[44] T. Hagiwara, Recent progress of photo-resin for rapid prototyping, "resin for stereolithography", *Macromolecular Symposia* **2001**, *175*, 397-402.
[45] G. A. Brady, J.W. Halloran, Stereolithography of ceramic suspensions, *Rapid Prototyping Journal* **1997**, *3(2)*, 61-65.
[46] X. Zhang, X.N. Jiang, C. Sun, Micro-stereolithography of polymeric and ceramic microstructures, *Sensors and Actuators A* **1999**, *77*, 149-156.
[47] F. Doreau, C. Caput, T. Chartier, Stereolithography for Manufacturing Ceramic parts, *Advanced Engineering Materials* **2000**, *2(8)*, 493-496.
[48] T. Chartier, C. Caput, F. Doreau, M. Loiseau, Stereolithography of structural complex ceramic parts, *Journal of Materials Science* **2002**, *37*, 3141-3147.
[49] A. Bertsch, S. Jiguet, P. Renaud, Microfabrication of ceramic components by microstereolithography, *Journal of Micromechanics and Microengineering* **2004**, *14(2)*, 197-203.
[50] A. Bertsch, S. Jiguet, H. Hofmann, P. Renaud, Ceramic microcomponents by microstereolithography, I*EEE International Conference on Micro Electro Mechanical Systems*, Technical Digest, 17th, Maastricht, Netherlands, Jan. 25.-29. 2004, pp 725-728, Institute of Electrical and Electronics Engineers, New York, N. Y., USA, ISBN: 0-7803-8265-X, **2004**.
[51] T. Chartier, C. Hinczewski, S. Corbel, UV curable systems for tape casting, *Journal of the European Ceramic Society* **1999**, *19*, 67-74.
[52] J.W. Lee, I.H. Lee, D.-W Cho, Development of micro-stereolithography technology using metal powder, *Microelectronic Engineering* **2006**, *83*, 1253-1256.
[53] Y.-W. Wang, C.-T. Yen, W.-C. Chen, Photosensitive polyimide/silica hybrid optical materials: Synthesis, properties and patterning, *Polymer* **2005**, *46*, 6959-6967.
[54] P. Dickinson, M. Ellwood, Water-based photopolymerizable compositions and their use, *GB P 2137626*, **1983**.
[55] E. A. Fohrenkamm, A. D. Rousseau, Ethylenically-unsaturated dextrin composition for preparing a durable hydrophilic photopolymer, *US P 4511646*, **1985**.
[56] R. Houbertz, Laser interaction in sol-gel based materials - 3D lithography for photonic applications, *Applied Surface Science* **2005**, *247*, 504-512.